High Precision Control of Magnetically Driven Microtools for Cell Manipulations

Masaya Hagiwara, Tomohiro Kawahara, Yoko Yamanishi, Beom H. Lee, and Fumihito Arai

Abstract – This paper presents two innovative driving methodologies using magnetically driven microtools for precise cell manipulations and its automation systems. First, the magnetic analysis has been conducted to show the current MMT problem. Then, the new driving methodologies are introduced and backed up with FEM analysis and the experimental results. The positioning accuracy improves 3-10 times and the following response become 10 times higher against the driving linear stage. Using this methodology, the enucleation of oocytes is demonstrated to show the effectiveness of the method.

I. Introduction

Cell manipulations in the confined space of a microfluidic chip are highly important in the field of biotechnology because of the low contamination capability, repeatability, and high throughput ability. A considerable amount of research has been carried out on magnetic actuators because of their non-contact drive, low invasiveness with respect to a cell, and low production cost [1-4]. In a previous study, we developed polymer-based magnetically driven microtools (MMTs) for cell manipulation, as well as stirrer, valve, droplet generation, etc.; these microtools were controlled by the applied magnetic fields [5-7]. However, the actuations were only an on-off control, and positioning accuracy was not required. In order to achieve positioning control, pairs of Helmholtz coils have been used in some research [8-10], but the supplied force by magnetic coil is not sufficiently strong to manipulate a relatively large cell such as an oocyte. Many cell manipulations require a force in the order of submillinewtons to millinewtons while a magnetic coil cannot output such a high power unless the magnetic coil is huge or a high voltage is applied. On the other hand, a permanent magnet has a more than 10 times stronger magnetic field to drive an MMT than an electromagnetic coil of the same size. Gauthier et al. proposed the precise control of magnetic objects using a permanent magnet [11], but its principle can be applied only when the size of the driven object has to be much small comparing to the drive magnet and thus the output force is quite small or the drive unit is huge.

When an MMT is driven by a permanent magnet on the XY stages from beneath the chip, there is an area where the MMT is not driven when the magnet passes under the MMT; we call this area the "dead band". Figure 1 shows an MMT (diameter: 1.0 mm) made of Ni and driven by a commercialized

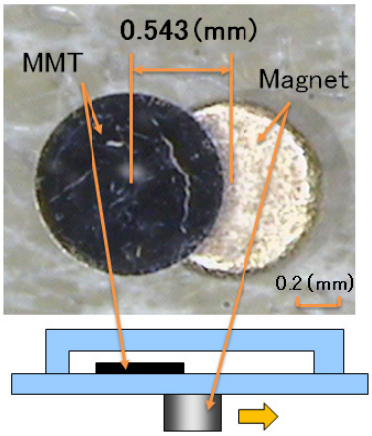

Fig. 1. Measured dead band area when MMT is driven by a permanent magnet (magnet: Neodymium, ϕ 1.0 mm x 0.05 mm, MMT: Ni, ϕ 1.0 mm x 1.0 mm)

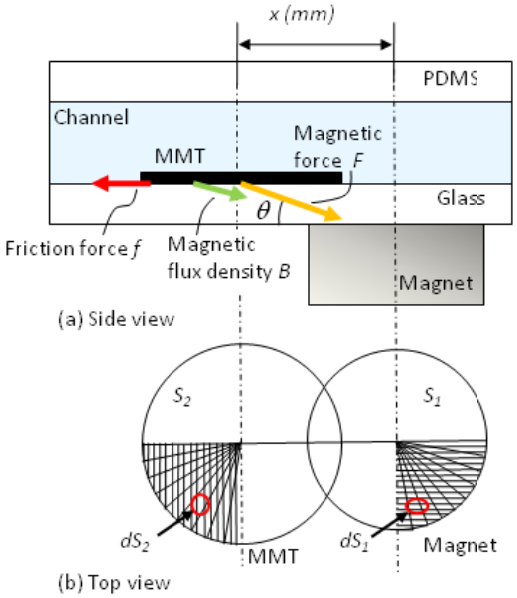

Fig. 2.Static force model driven by a permanent magnet in a chip

Manuscript received March, 2010. This work was supported in part by JST-Sentan project.

M. Hagiwara is with Department of Mechanical Science & Engineering, Nagoya University, Nagoya, 464-8603 Japan (phone: +81-52-789-5656; fax: +81-52-789-5213; e-mail: hagiwara@biorobotics.mech.nagoya-u.ac.jp).

T. Kawahara is with Department of Mechanical Science & Engineering, Nagoya University, Nagoya, 464-8603 Japan (phone: +81-52-789-5656; fax: +81-52-789-5213; e-mail: tkawahara@mech.nagoya-u.ac.jp).

Y. Yamanishi is with JST PRESTO Nagoya, 464-8603 Japan phone: +81-52-789-5656; fax: +81-52-789-5213; e-mail: yoko@mech.nagoya-u.ac.jp)

Beom H. Lee is with Seoul National University, Seoul, Korea (email: bhlee@snu.ac.jp)

F. Arai is with with Department of Mechanical Science & Engineering, Nagoya University, Nagoya, 464-8603 Japan (phone: +81-52-789-5025; fax: +81-52-789-5213; e-mail:arai@mech.nagoya-u.ac.jp).

neodymium ($Nd_2Fe_{14}B$) permanent magnet (diameter: 1.0 mm, grade: N40). This MMT is not driven until the distance between the magnet and MMT is approximately 500 µm, and then the MMT starts following the magnet. The dead band interferes with the precise positioning of the MMT on a chip and deteriorates the effective control of MMT as a robot on a chip because of the slow response speed to the driver unit. Therefore, we present a dead band analysis to find out the root cause of the low sensitivity and introduce an effective driving methodology to counter this cause for precisely controlling an MMT with large force output that is driven by permanent magnets.

II. Dead Band Analysis

In order to counter the cause of the dead band and predict its amount for a certain MMT and a magnet, we have developed a static force model on the MMT (Figure 2). The gravitational force, buoyant force, and the Van der Waals' force are ignored in this model since these are relatively small as compared to the magnetic force applied to the MMT. For the calculation of the magnet force, the magnet and the MMT are subdivided into very small elemental areas dS_1 and dS_2, respectively. Then, the vector $\boldsymbol{B}$, which is the magnetic flux density in the small elemental area of the MMT (dS_2), can be computed by dividing the sum of the vectors of the flux from each small elemental area dS_1 by the magnet area S_1.

$$\vec{B} = \iint d\vec{B} \cdot dS_1 \Big/ S_1 \qquad (1)$$

where $\boldsymbol{dB}$ is the flux density from each small elemental area of the magnet dS_2. However, it is quite difficult to express the magnetic flux density distribution around a magnet by single formula since the magnetic flux density $\boldsymbol{B}$ has the complicated nonlinear distribution due to its dependence of size, shape, and the magnet material feature. Therefore, the cubic spline interpolation from measured data is used to predict the magnetic flux density distribution around the magnet.

The elemental force $\boldsymbol{dF}$ caused by $\boldsymbol{B}$ can be expressed in the same manner as that analyzed by Abbott *et al.* [12]. That is,

$$d\vec{F} = \upsilon(M \cdot \nabla)\vec{B} \qquad (2)$$

where v is the MMT volume, and M is the magnetization. In high magnetization region, M can be approximated by the saturation magnetization. The total magnetic force $\boldsymbol{F}$ on MMT can be calculated by the sum of the elemental forces $\boldsymbol{dF}$ as follows;

$$\vec{F} = \iint d\vec{F} \cdot dS_2 \qquad (3)$$

The drive force of the MMT is the horizontal component of $\boldsymbol{F}$; further, the maximum static friction force f on the MMT can be expressed as the product of the vertical component of $\boldsymbol{F}$ and the static friction coefficient μ. The MMT can move when the drive force is larger than the maximum static friction force:

$$\left|\vec{F}\right|\cos\theta - \left|\vec{F}\right|\sin\theta \times \mu > 0 \qquad (4)$$

where θ is angle between $\boldsymbol{F}$ and a horizontal line.

Figure 3 shows the simulation result under the conditions that the magnet size is ϕ1.0 x 1.0 mm, and the material is Neodymium, while the MMT size is ϕ1.0 x 0.05 mm, and the material is nickel. The saturation magnetization is material constant, which is 5.12 x 10^5 A/m for Ni. It can be seen that the magnetic force in horizontal direction increases along with the distance increase around the magnet, and then starts decreasing with increasing distance, while the maximum static friction force is almost constant around the magnet and starts decreasing with increasing distance. In the region,

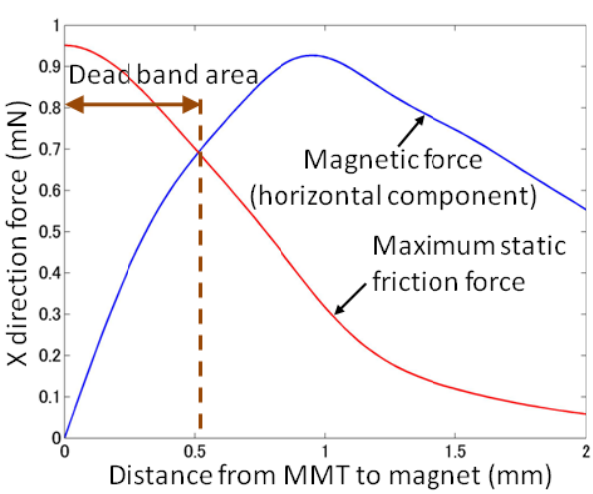

Fig. 3. Simulation result of the drive force of MMT and the friction force (magnet: Neodymium, ϕ 1.0 mm x 0.05 mm, MMT: Ni, ϕ 1.0 mm x 1.0 mm)

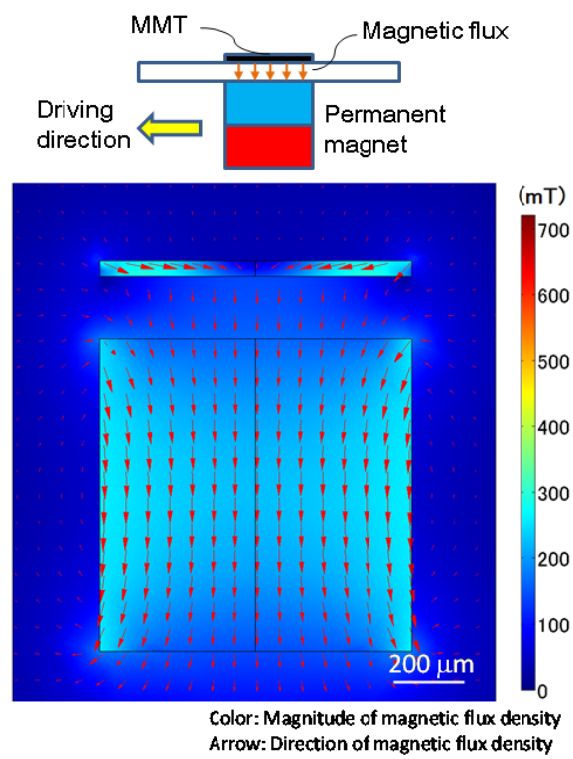

Figure 4. FEM result of magnetic flux density (magnet: Neodymium, ϕ 1.0mm, MMT: Ni, ϕ 1.0mm)

where the magnet is totally covered by the MMT, the friction force is higher than the drive force. Thus, the MMT does not move in this region in spite of the magnet movement. When the distance reaches to 513.0 μm, the drive force exceeds the friction force and the MMT starts following to the magnet. This simulation result is corresponding to the measured dead band amount mentioned above (543.0 μm).

From this result, it can be determined that the dead band is caused by the static friction. This simulation can predict the drive force, the required force to drive the MMT and the dead band amount respectively and helps designing the magnetic microactuators to avoid dead band. And now that it is clear that the cause of the low positioning accuracy and controllability is the static friction, next stage is how to reduce the friction on the MMT.

III. Low Friction Drive Units

Figure 4 shows the magnetic flux density distributions by an FEM analysis for ϕ1.0 x 1.0 mm under the ϕ1.0 x 0.05 mm Ni MMT. As shown in the figure, the direction of the magnetic flux density around Ni MMT is vertically aligned and thus the large magnetic force to downward direction is applied. This makes the friction on an MMT by conventional drive larger. Two effective drive methods to reduce the friction on an MMT are proposed as following.

(a) Two-tiered magnetic drive (TMD)

In order to reduce the friction, the vertical force on an MMT has to be reduced. Figure 5(a) shows the concept of two-tiered magnetic drive (TMD). The magnetic sheet, which is embedded in a microfluidic chip, counters the magnetic flux of the drive magnet by applying magnetic flux in reverse direction. Since an MMT is subject to both of upward and downward force, it leans in a microchip and thus the contact area between the MMT and the grass substrate is significantly reduced. In order to minimize the vertical force on an MMT, it would be better to use the magnet sheet and the drive magnet with the similar magnetic strength.

Figure 5(b) shows the FEM result for ϕ1.0 x 1.0 mm under the ϕ1.0 x 0.05 mm Ni. Comparing with Figure 4, the magnetic flux around the MMT, which is aligned along the vertical direction, decreases. Much reduced downward force and smaller contact area makes the friction drastically reduced.

(b)Horizontal polar driving unit (HPD)

Another way to reduce the vertical force on the MMT is that the MMT is set such that the permanent magnet pole is parallel to the driving direction of a magnet that has the same size as the MMT. Here we describe the driving method of the MMT in such setup as the horizontal polar drive (HPD). Figure 6 shows the concept and the FEM result of HPD. The magnetic flux flows in a circular pattern through the MMT, and its direction is aligned to the driving direction. As a result, there is considerably less magnetic flux in the vertical direction around the center of the MMT as compared to that shown in Figure 4. This implies that magnetic power with a

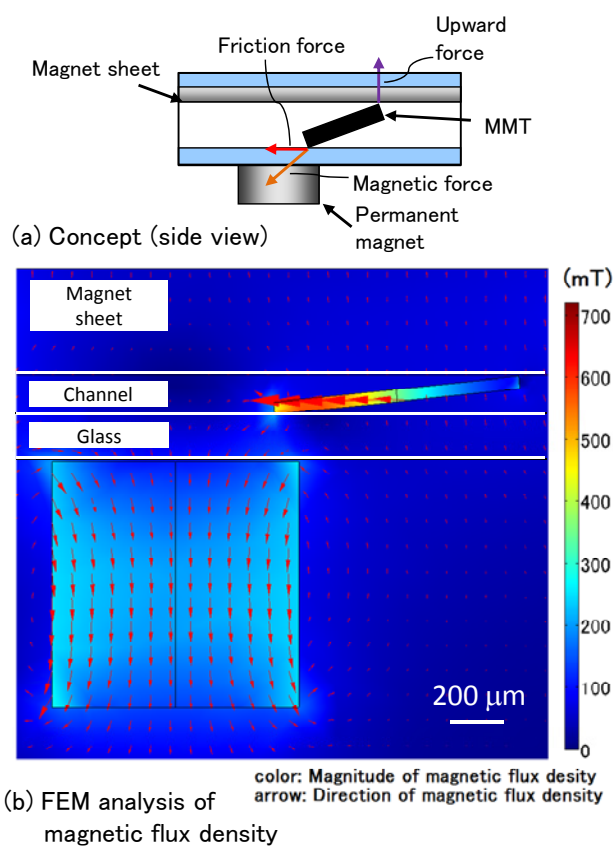

Figure 5. Two-tiered magnetic drive

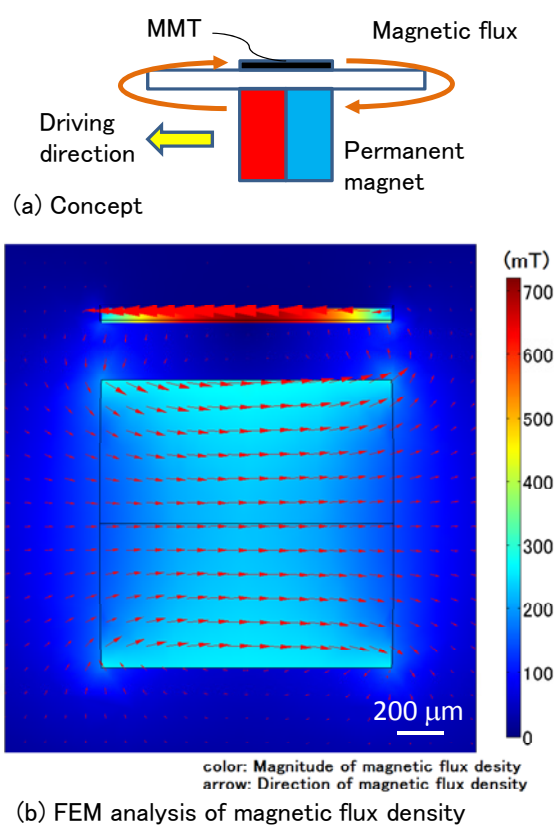

Figure 6. Horizontal polar drive

considerably high efficiency is applied to the MMT and the magnetic force on the MMT is much greater in the driving direction than in the vertical direction; therefore, the friction force is reduced by decreasing the vertical force on the MMT.

IV. Experimental Evaluations

The experiment has been conducted to evaluate two driving methods, TMD and HPD. Figure 7 shows the experimental set up including the linear stage for the magnet actuation, the microscope with CCD camera, and PC for controlling the stage and capturing image data from CCD camera. Ni based ϕ 1.0 mm x 0.05 mm circular disc is used as an MMT and a neodymium based ϕ 1.0 mm x 1.0 mm cylinder magnet is used as a drive unit. The magnet is commercially available and its surface magnetic flux density is 166 mT (grade: N40).

Figure 8 shows the experimentally obtained following response ability of the MMT against the linear stage with the permanent magnet. The stage moves in 1 degree of freedom (DOF) with 0.5 Hz sine wave and the stroke is ±1.4 mm. In the case of conventional drive, the movement of the MMT against the stage is delayed by 0.3 sec; the maximum difference between the MMT and the stage is 1.0 mm. Under this large time lag, the MMT cannot respond to the cell movement in a microfluidic chip and this makes the development of an automation system difficult. On the other hand, in both of the TMD and HPD, the response of the MMT is more than 10 times faster. Figure 9 shows the comparison of the MMT positioning error against the drive magnet. Comparing to the positioning error in the conventional drive, the average error is 5 times smaller in TMD and 10 times smaller in HPD. Precise positioning accuracy and following response to stage are essential for developing automation systems as well as the manipulation of small size of objects.

In the meanwhile, the difference between the stage and the MMT tends to get worse around the returning points, which is the stage speeds smaller. This result implies that the friction on the MMT has velocity dependence. According to the Stribeck curve in fluid lubrication field, in boundary lubrication region or mixed film lubrication region, where the liquid film thickness is smaller than surface roughness of the MMT, the more the velocity increases, the more liquid film thickness increases [13]. And as a result, the friction decreases. Therefore, the friction on the MMT exceeds the drive force around the returning point since the velocity is close to zero and the MMT start delaying to the stage.

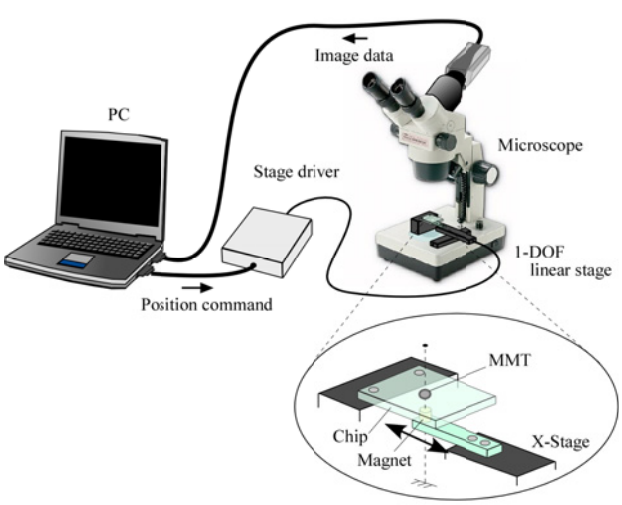

Fig.7. Experimental set up

V. Enucleation of Oocytes

Now, we introduce the enucleation of oocytes process in a microfluidic chip by MMTs applying HPD to prove its availability. The enucleation of oocyte is needed for cloning process. At present, manually operated micromanipulators with glass capillaries are used to remove a nucleus under a microscope. However, the conventional manual manipulation tends to have problems of contamination, low success rate and low repeatability, and thus complicated cell manipulation could be carried out only by skilled people. Automation of the

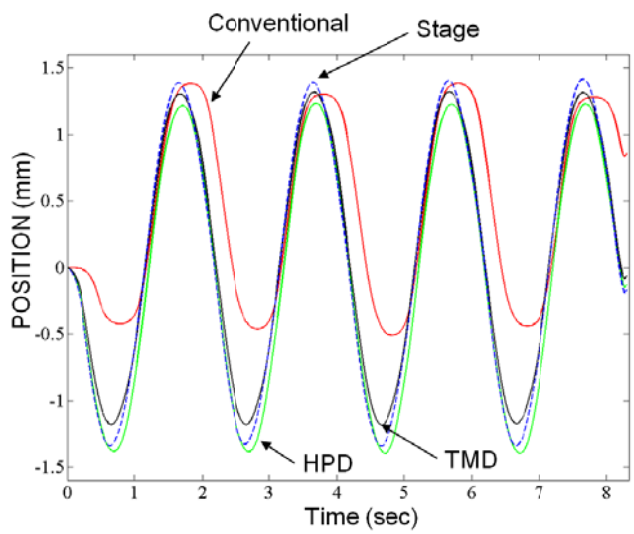

Fig.8. Following response of the MMT to the linear stage using 3 different driving unit (Ni based MMT: ϕ 1.0 mm x 0.05 mm, neodymium magnet: ϕ 1.0 mm x 1.0 mm)

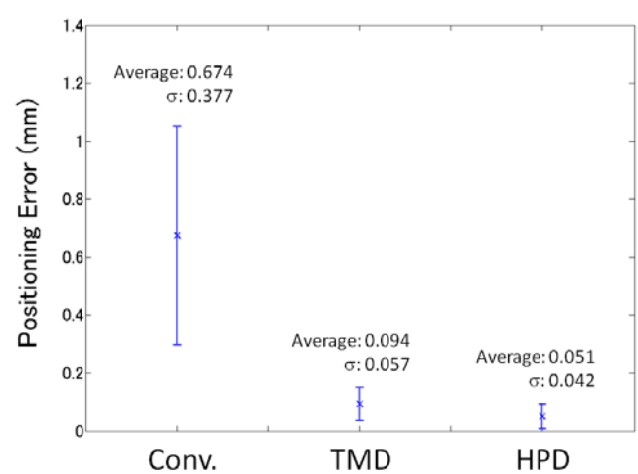

Fig.9. Positioning error between the drive magnet on the linear stage and each drive method

cloning technique is required for high-throughput production of processed cells with high quality and homogeneity [14]. The approach to enucleate oocytes in a microfluidic chip using hybrid MMTs was conducted previously [15], but it was quite difficult to develop the automation system since the positioning error between the stage and the MMT was too big to control. Besides, it was difficult to handle continuously moving cell due to the slow response of the MMT against the drive stage. Here, we have conducted the enucleation process on a chip with fast response by HPD.

Figure 10 shows the design of the microfluidic chip for the enucleation of oocytes. The cutting blade has to have enough power to cut the oocytes and precise positioning is required to aim at the target properly. Two MMT blades made by Ni, whose young's module is enough higher than oocyte's (50 GPa), is set in polydimthysiloxane (PDMS) chip to cut off the oocytes at the middle of the chip. The oocytes are put in from inlet port and flow in 200 μm height and width of the channel. The channel height is set lower at the intersection of the channel and the MMT pathway not to escape oocytes from the cutting blades by squeezing them. The channel width to the outlet narrows to 50 μm to prevent the oocytes from evacuating without cutting.

The Ni based MMT fabrication process is shown in Figure 11. At first, the sacrificial layer (LOR 5B, Tokyo Ohka Kogyo Co., Ltd.) is coated on Si wafer. Then Cr-Au is sputtered on this wafer (thickness = 300 nm). Next, the photoresist (KMPR 3035, Nippon Kayaku Co., Ltd.) is coated on the substrate. After the exposure, the KMPR pattern is developed. Finally the Ni was grown by the electroplating (= 50 μm). After removing the photoresist and sacrificial layer, the Ni parts can be collected and cleaned by ultrasonic. The tip of the blade for enucleation has been sharpened to cut off oocytes easily and 1000 μm length square part has been designed to make an MMT powerful enough to cut oocytes.

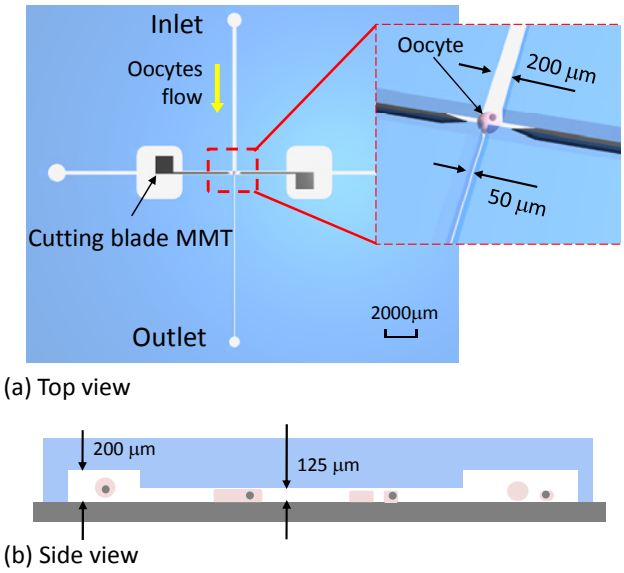

Fig.10. Design of microfluidic chip for enucleation of oocyte

The center of the square part is not aligned to the blade axis to avoid interfering with each stage and magnetic field. The thickness of the MMT is 50 μm to have enough clearance in the channel.

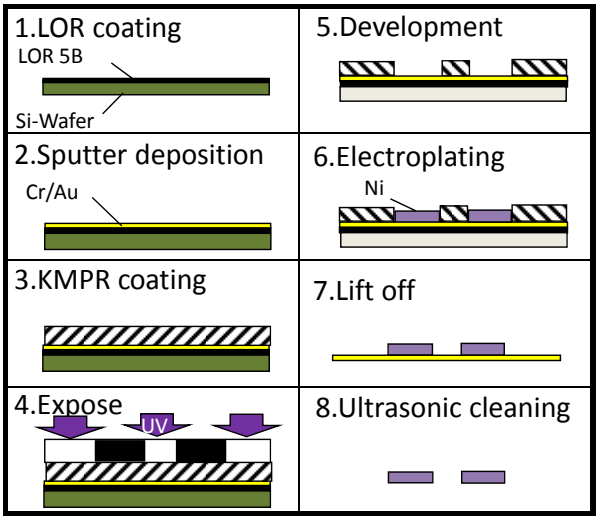

(a) MMT fabrication process

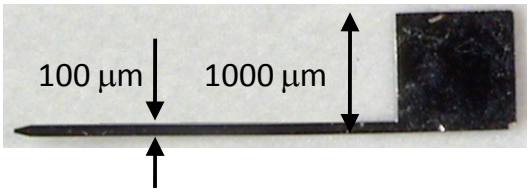

(b) Cutting blade MMT shape and size

Fig.11. Fabrication process of Ni based MMT for enucleation operation

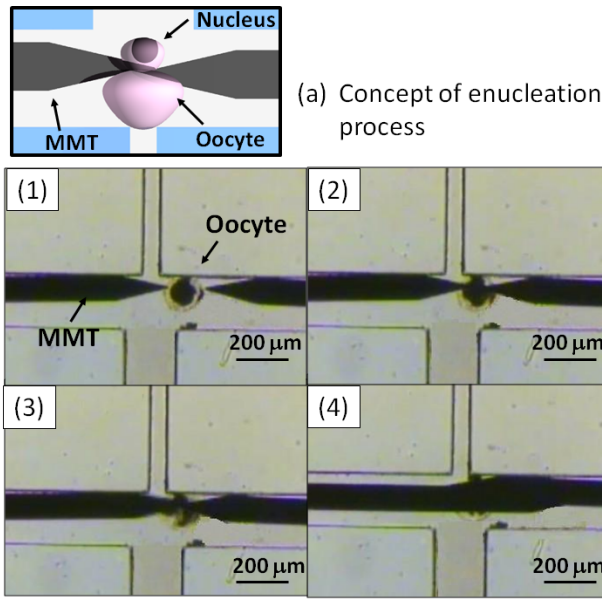

(b) Enucleation process sequence

Fig.12. Enucleation of oocytes process in microfluidic chip by MMT with horizontal polar drive

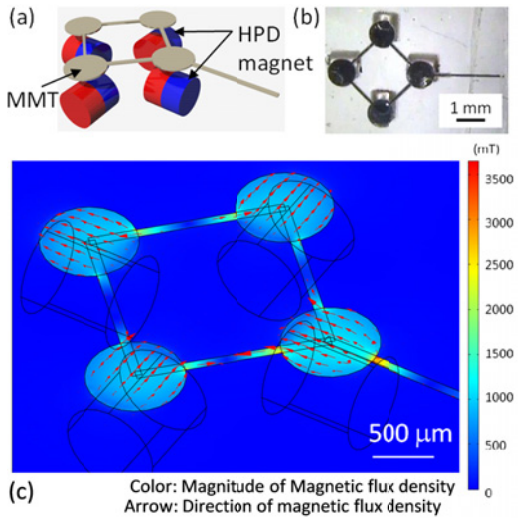

Fig.13. Two-DOF MMT with HPD magnet. (a) Concept, (b) actual design and (c) FEM result of magnetic flux density (magnet: neodymium, ϕ 1.0 mm × 1.0 mm, MMT: Ni).

The HPD method is used to achieve the positioning accuracy and the same permanent magnet as the fundamental experiment mentioned above is used (neodymium ϕ 1.0 mm x 1.0 mm). Because of the fast response speeds of the blade MMT using HPD, the MMT can move up to 5 Hz, which is the linear stage speed limit. Figure 12 shows the actual cutting process under the conditions mentioned above. Oocyte comes from inlet with water and reaches to the intersection with squeezed. Owing to the rapid response of the MMT to the stage and the high resolution of the MMT positioning accuracy using HPD, the cutting blade can aim at the oocyte properly with ease, and thus, the throughput of the enucleation process has dramatically increased.

VI. Conclusions

Two distinguished driving methods to increase the positioning accuracy and the response speeds of MMT by reducing friction force are presented and their effectiveness is proved analytically and experimentally. The capability of the HPD has been shown in enucleation process in this paper, but it is also useful for other process of MMT such as sorting cell particle process to multiple branches. However, these capabilities of both of TMD and HPD are available only on 1 degree of freedom. In order to develop the HPD to multi-degree of freedom, assembling the magnets with the HPD conditions is effective. Figure 13 shows the concept of the multi-DOF MMT using HPD [16]. The evaluations of the accuracy and refining the positioning accuracy more precisely are our future work.

VII. Acknowledgement

This research is supported by JST-Sentan program.

References

[1] G. A. Mensing, T. M. Pearce, M. D. Graham, and D. J. Beebe, "An externally driven magnetic microstirrer", Phil. Trans. R. Soc. London, Ser.A, vol. 362, pp. 1059-1068, 2004.

[2] M. Barbic, J. J. Mock, A. P. Gray, and S. Schults, "Electromagnetic micromotor for microfluidics applications", Applied Physics Letters, vol. 79, No. 9, pp. 1399-1402, 2001.

[3] M. Roper, R. Dreyfus, J. Baudry, M. Fermigier, J. Bibette, and H. A. Stone, "On the dynamics of magnetically driven elastic filaments", Journal of Fluid Mechanics, vol. 554, pp. 167-190, 2006.

[4] D. C. Meeker, E. H. Maslen, R. C. Ritter, and F. M. Creighton, "Optimal realization of arbitrary forces in a magnetic stereotaxis system", IEEE Transactions on Magnetics, vol. 32, No. 2, pp. 320-328, 1996.

[5] Y. Yamanishi, S. Sakuma, K. Onda, and F. Arai, "Powerful Actuation of Magnetized Microtools by Focused Magnetic Field for Particle Sorting in a Chip", Biomed Microdevices, vol. 12, pp. 745-752, 2010

[6] Y. Yamanishi, Y. Kihara, S. Sakuma, and F. Arai, "On-demand production of emulsion droplets using hybrid magnetically driven microtool", International Journal of Automation Technology, vol. 3, pp.502-508, 2009.

[7] N. Inomata, Y. Yamanishi, and F. Arai, "Manipulation and observation of carbon nanotubes in water under an optical microscope using a microfluidic chip", IEEE international symposium on micro-nanomechatronics and human science, pp. 493-398, 2009.

[8] C. Pawashe, S. Floyd, and M. Sitti, "Modeling and experimental characterization of an untethered magnetic micro-robot", International Journal of Robotics Research, vol. 28, pp. 1077-1095, 2009.

[9] M. S. Sakar, E. B. Steager, D. H. Kim, M. J. Kim, G. J. Pappas, and Vigay Kumar, "Single cell manipulation using ferromagnetic composite microtransporters", Applied physics letters, vol. 96, issue. 4, pp.96-98, 2010.

[10] J. J. Abott, K. E. Peyer, M. C. Lagomarsino, L. Zhang, L. Dong, I. K. Kaliakatsos, and B. J. Nelson, "How should microrobots swim?", The international journal of Robotics Research, vol. 28, pp. 1434-1448, 2009.

[11] M. Gauthier, and E. Piat, "An electromagnetic micromanipulation system for single-cell manipulation", Journal of Micromechatronics, vol. 2, No. 2, pp. 87-119, 2004.

[12] J. J. Abott, O. Ergeneman, M. P. Kummer, A. M. Hirt, and B. J. Nelson, "Modeling magnetic torque and force for controlled manipulation of soft-magnetic bodies", IEEE Trans. on Robotics, vol. 23, No. 6, pp.1247-1252, 2007.

[13] Y. Ando, "Introduction to microtribology", Yoneda

[14] Y. Yamanishi, T. Mizunuma, N. Inomata, S. Kudo, and F. Arai, "Soft scrubbing off of zona pellucid on disposable microfluidic chip", IEEE the 24th international conference on micro electro mechanical systems, pp. 256-259, 2010.

[15] N. Inomata, T. Mizunuma, Y. Yamanishi, S. Kudo, and F. Arai, "On-chip magnetically driven micro-robot for enucleation of oocyte", IEEE international symposium on micro-nanomechatronics and human science, p. 493-496, 2009.

[16] M. Hagiwara, T. Kawahara, Y. Yamanishi, and F. Arai, "Driving Method of Microtool by Horizontally-arranged Permanent Magnets for Single Cell Manipulation", Applied Physics Letters, vol. 97, pp. 013701-1 -013701-3, 2010.